

Article

Development of a Biocompatible Layer-by-Layer Film System Using Aptamer Technology for Smart Material Applications

Amanda Foster and Maria C. DeRosa *

Department of Chemistry, Carleton University, Ottawa-Carleton Chemistry Institute,
1125 Colonel By Drive, Ottawa, ON, K1S 5B6, Canada; E-Mail: amandafoster115@gmail.com

* Author to whom correspondence should be addressed; E-Mail: maria.derosa@carleton.ca;
Tel.: +1-613-520-2600 (ext. 3844); Fax: +1-613-520-3749.

Received: 17 March 2014; in revised form: 4 May 2014 / Accepted: 8 May 2014 /

Published: 23 May 2014

Abstract: Aptamers are short, single-stranded nucleic acids that fold into well-defined three dimensional (3D) structures that allow for binding to a target molecule with affinities and specificities that can rival or in some cases exceed those of antibodies. The compatibility of aptamers with nanostructures such as thin films, in combination with their affinity, selectivity, and conformational changes upon target interaction, could set the foundation for the development of novel smart materials. In this study, the development of a biocompatible aptamer-polyelectrolyte film system was investigated using a layer-by-layer approach. Using fluorescence microscopy, we demonstrated the ability of the sulforhodamine B aptamer to bind its cognate target while sequestered in a chitosan-hyaluronan film matrix. Studies using Ultraviolet-visible (UV-Vis) spectrophotometry also suggest that deposition conditions such as rinsing time and volume play a strong role in the internal film interactions and growth mechanisms of chitosan-hyaluronan films. The continued study and development of aptamer-functionalized thin films provides endless new opportunities for novel smart materials and has the potential to revolutionize the field of controlled release.

Keywords: aptamer; sulforhodamine B; layer-by-layer; chitosan; hyaluronan; exponential growth; linear growth; polyelectrolyte

1. Introduction

Layer-by-layer (LBL) assembly was first described by Decher in the 1990s as an alternative method to Langmuir-Blodgett (LB) assembly for the fabrication of thin films [1]. LB assembly allows for the fabrication of multilayers using primarily amphiphilic molecules with alternating head-to-head/tail-to-tail arrangement and has been extensively reviewed [2–4]. Despite being able to produce multilayer films, the technique itself is time consuming, requires expensive equipment to perform and is limited by the type of molecules that can be used. The advent of LBL assembly enabled many of these limitations to be overcome, and as a result it has become a popular approach to multilayer assembly [5–9]. Using this method, polyelectrolyte multilayers (PEMs) are fabricated by sequential, alternating adsorption of negatively and positively charged polymers (polyelectrolytes, PE) onto a charged substrate. Each monomer unit of a PE possesses a charge, creating a multiply-charged molecule in which electrostatic interactions are possible [10]. Other interactions (although less common) can also drive PEM formation including hydrogen bonding [11], coordination chemistry [12], and hydrophobic interactions [13]. Therefore, LBL assembly offers a simple method of PEM preparation without the same material limitations of LB assembly, requiring minimal equipment to perform while maintaining nanoscale control over film preparation.

From this, PEs can be sorted into two groups: those with permanent charges in solution (strong PE) and those whose charge depends strongly on pH (weak PE) [10]. The charge density—based on the number of groups composing the repeating monomer unit—will also influence the interactions possible between PEs [14]. The nature of the PEs (*i.e.*, charge density, molecular weight, weak *versus* strong) will strongly influence the behavior of the resulting film. LBL films are mainly held together by electrostatic interactions. Charges within the film are neutralized intrinsically or extrinsically [10]. Intrinsic charge compensation refers to the pairing of charges between the PEs, while charges neutralized by extrinsic compensation are paired with a counter-ion from the surrounding solution. Fixed charges are charges within the film that cannot be paired with a charge from another PE due to imposed constraints from the film structure, *i.e.*, sterics—these rely on neutralization through extrinsic compensation [15].

The earliest models of PEM growth show linearly growing systems where the increase in mass and film thickness is proportional to the number of deposited bilayers (deposition steps). Indeed, there are many examples of linearly growing films involving synthetic and natural PE including poly(sodium styrene sulfonate) (PSS)/poly(allyamine hydrochloride)(PAH) [16] and chitosan (CHI)/cellulose nanowhiskers [17] films. In these films, each bilayer interacts only with bilayers that directly neighbor it (above or below) with very little inter-penetration and as a result, a distinct layered morphology is seen within the film [15,18]. However, more recent studies—such as those done by Elbert *et al.* using poly(L-lysine) (PLL) and polyethylimine, and Picart *et al.* using PLL and hyaluronan (HA)—demonstrated film systems that did not adhere to this growth mechanism [19,20]. Rather, these systems showed exponential increases in film thickness with each deposition cycle. This type of growth was attributed to a diffusion model where at least one PE is able to move in and out of the film during buildup (See Figure S1). Generally, films which grow by this mechanism are composed of natural polymers. However, linear and exponentially growing films are interrelated. The experimental conditions (*i.e.*, temperature, pH, ionic concentration) under which a film is constructed

play a large role in the resulting interaction strength between the PEs involved, and in turn influence the growth mechanism, density, and strength of a given film [10]. These parameters are just as important as the nature of the PEs themselves (*i.e.*, weak *versus* strong, molecular mass, 2° interactions) for determining film behavior. Linearly-growing films tend to favor highly charged PE and low ionic strength conditions where intrinsic charge compensation is dominant, forming dense film structures [10,15]. However, if the ionic strength is increased, the growth mechanism can be changed to exhibit exponential behavior. This was seen when PSS/PAH films constructed in 1 M NaCl grew exponentially while those built in 0.15 M NaCl grew linearly [21,22]. It has been observed in reverse as well; characteristic exponential growth can be reverted to linear growth by decreasing the ionic strength. For example, CHI/HA films grew linearly in 10^{-4} M NaCl but grew exponentially at concentrations of 0.15 M NaCl [18]. However, films exhibiting exponential growth tend to be unstable at low ionic strengths and there are structural repercussions to deposition under these conditions. For example, CHI/HA films deposited in 10^{-4} M NaCl cannot form continuous films and remain as islands [18].

LBL films are created through an iterative procedure where a substrate is dipped into polyelectrolyte solutions of opposite charge with an intermediate rinsing step in between to prevent cross-contamination between solutions (See Figure S2). Many studies have focused on the effects of varying conditional parameters such as pH [23,24], temperature [25], and ionic strength [10,18,21,22,26], however no work has been performed to determine the effects of the intermediate rinsing step on film growth. In addition to this, while there are many cases of linear-to-exponential transitions as a result of experimental conditions, very few cases have been reported of the opposite in the early stages of deposition (within the first 10–15 layers) where the integrity and continuity of the film are not affected. Therefore, the first section of this study focuses on the effect of varying the rinsing conditions on LBL film growth. Films composed of CHI and HA were chosen for this work. These films typically display exponential growth and have been characterized extensively in respect to growth mechanism, growth rate, and film behavior [18,27–29].

In recent years, aptamers—which are short, single-stranded nucleic acids that fold into well-defined three dimensional (3D) structures and possess the ability to bind a target with high specificity and selectivity—have proven very promising in the field of molecular recognition. They are also very compatible with nanomaterials and have been used to grant the advantages of their binding properties to materials in many applications including hydrogels [30], nanoparticles [31], liposomes [32], micelles [33], and carbon nanotubes [34], mainly for the purpose of controlled delivery, sensing, and therapeutics. Together, the combined properties of aptamers and nanomaterials may provide the technological advance to create dynamic materials that are responsive to the surrounding environment—hence “smart” nanomaterials [35].

Surprisingly, limited work has been performed using aptamers in LBL films with the first reports being the proof-of-concept for the studies discussed in this work. LBL assembly is highly suited for the integration of aptamers into PEMs; using the negatively charged backbone, the DNA can interact electrostatically with the chosen PEs to create the desired film. However, there are inherent challenges to integrating aptamers into a confined film matrix. The matrix must not interfere with aptamer folding and the final conformation must be correct in order to retain the binding properties of the aptamer. The target must also be able to permeate the matrix to access the aptamer. Both of these challenges were overcome by Sultan *et al.* who functionalized PSS/PDDA (PDDA: poly(diallyldimethylammonium

chloride)) films and PSS/PAH microcapsules using the sulforhodamine B aptamer (SA) [36,37]. Sequestering SA within a PSS/PDDA film only had a modest effect on the aptamer K_d (0.7–16 μM) and aptamer films bound the target dye much more effectively than films prepared with other DNAs [36]. In a slightly different system, the flux of small molecules across PSS/PAH/SA microcapsule walls could be altered by aptamer-target interaction [37]. Both studies demonstrate the value of LBL aptamer film systems. Several other systems have emerged recently as well. Malile *et al.* harnessed the morphological changes that can be induced in LBL films by target interaction with embedded aptamers to control the diffusion of an etchant across a PSS/PAH/aptamer film as part of a colorimetric detection platform using gold-coated nanoprisms [38]. In another detection platform, Du *et al.* used target interaction with LBL assembled aptamers to block the electrode surface on which they were assembled, giving a concentration-responsive dampening of the redox signal [39]. PSS/PDDA and PSS/PAH are excellent model systems for the study of novel nanomaterial applications however they fall short of the biocompatibility standards that are demanded of nanomaterials for practical applications. More recently, focus has shifted away from these synthetic systems and more towards natural polymer films which offer a promising new set of properties including biodegradability, biocompatibility, and lack of toxicity. Materials such as polysaccharides [18], polynucleotides [40], enzymes [41], polypeptides [21], and proteins [42] have been used to create novel films with different properties and functionalities. Thus, a new film model for use in aptamer-based materials, based on CHI and HA, was chosen to replace PSS and PAH. The behavior of polysaccharide films is quite different from synthetic systems with a new set of challenges and therefore the ability of an aptamer to function within this matrix must first be confirmed. The second section of this study describes the integration of the Sulforhodamine B (SB) aptamer into a CHI/HA film and the subsequent effect on binding function. The SB aptamer was chosen as it folds into a highly structured G-quadruplex conformation making it a good candidate to study the effects of a film matrix on aptamer function [26]. Therefore, the focus of this work was to determine whether aptamer technology can be expanded to other film systems which possess more of the desired properties for real-world applications (*i.e.*, biocompatibility). To explore this, the SB aptamer was integrated into films composed of CHI and HA polysaccharides and these novel films were evaluated for the interactions between the embedded aptamer and its target, SB dye. In addition to this, the changes in CHI/HA film growth with varying rinse protocols was also explored as an investigation of potential quality control concerns which need addressing.

2. Experimental Section

2.1. Materials

Glass (76 mm \times 25 mm) and quartz (50 mm \times 25 mm) microscope slides were purchased from VWR (Radnor, PA, USA). Gridded glass slides (75 mm \times 25 mm, 1 mm thick) were purchased from Lab Scientific (Livingston, NJ, USA). All slides were cut into smaller slides (\sim 1.5 mm \times 2.5 mm) using a hand-held diamond-tipped tool with exception of the grid slides which only had the excess glass surrounding the printed grid removed.

HA (M_w 1,580,000 Da) was purchased from Acros Organics (Geel, Belgium) as sodium hyaluronate. CHI (M_w 135,000 Da) was purchased from Acros Organics. SB dye was purchased from Sigma Aldrich (St. Louis, MO, USA). Phosphoramidites, modifiers, acetonitrile, deblock, activator, oxidizer, and capping reagents for DNA synthesis were purchased from Glen Research (Sterling, VA, USA). Columns (standard, 500 Å pore size) were purchased from BioAutomation (Kenning Court Plano, TX, USA). All purchased reagents were used as received.

The sulforhodamine B aptamer (SA sequence: 5'-CCG GCC TAG GGT GGG AGG GAG GGG GCC GG-3') and a random oligomer (RO) of the same length (RO sequence: 5'-GAC CTA TGA TAG CAT CAG TCG CAT CAG TC-3') were synthesized using standard phosphoramidite chemistry on a BioAutomation Mermade 6 DNA synthesizer as specified by the manufacturer. Modified SA and RO DNA was also prepared by adding fluorescein phosphoramidite (6-FAM) to the 5' end of the sequence.

All buffers were made with Milli-Q water and filtered with Corning 0.22 µm cellulose acetate filter units. Solution pH adjustments were made with diluted acetic acid. Glassware was rinsed five times with distilled and five times with deionized water prior to use. Deionized water was used for all experiments unless otherwise stated.

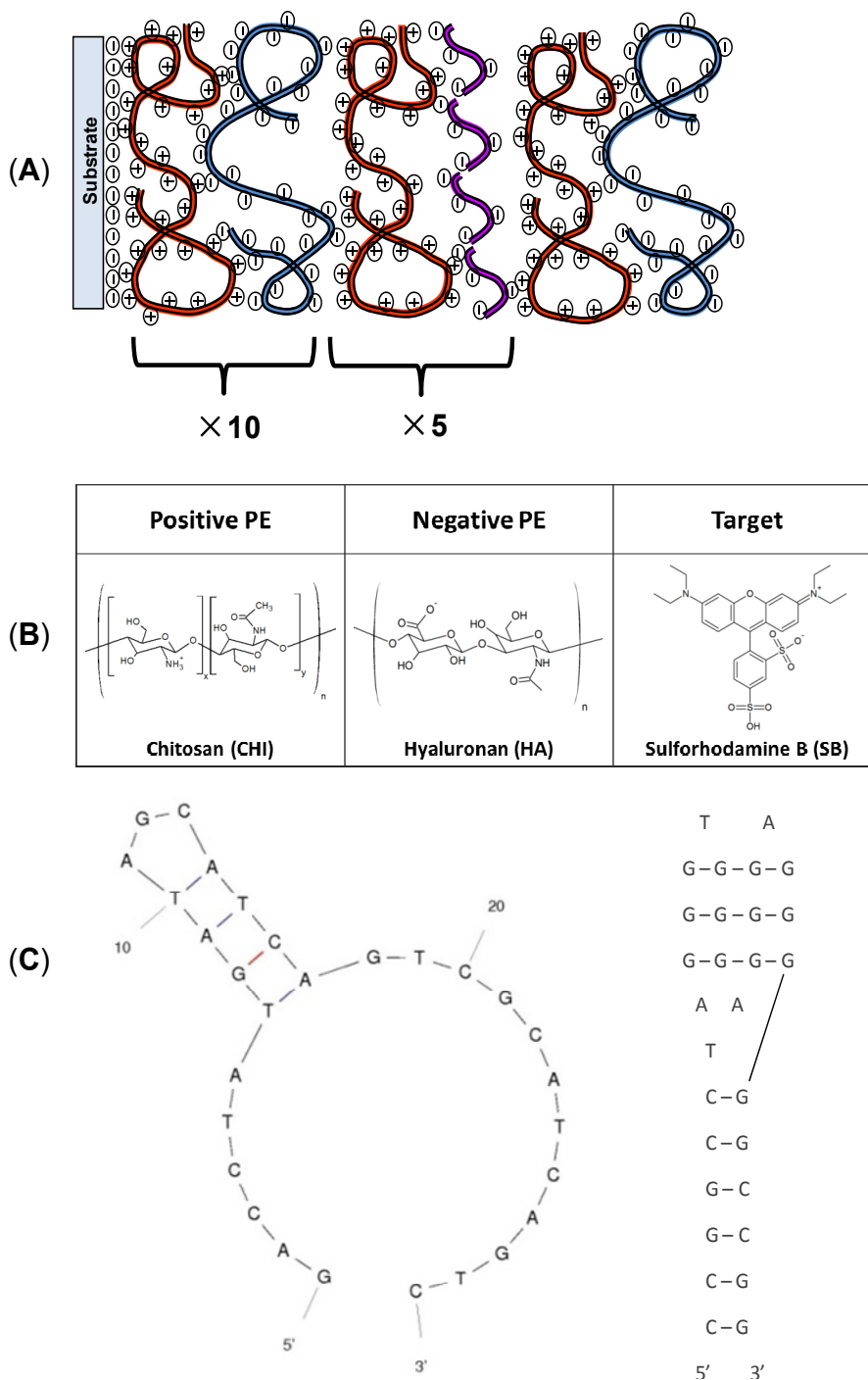
2.2. Film Deposition

Substrates (glass or quartz slides) were cleaned by incubating the slides in a 1:1:5 solution of $H_2O_2:NH_4OH:H_2O$ at 70–90 °C for ten minutes, followed by copious rinsing with water. Substrates were immediately used for film deposition.

Film solutions were prepared at 1 mg/mL in 0.15 M NaCl pH 4.5 unless otherwise stated. With a pK_a of ≈ 2.9 [29], HA is negatively charged at acidic pH. CHI has a pK_a of ≈ 6 [29] and therefore requires an acidic environment to become positively charged and also to dissolve in aqueous solution. The pHs of polyelectrolyte solutions were adjusted to 4.5 using diluted glacial acetic acid.

Cleaned slides were dipped successively in the CHI and HA (10 mL) solutions for 15 min each, with two rinses ($R_1 = 10$ s, 10 mL; $R_2 = 5$ s, 10 mL) in 0.15 M NaCl pH 4.5 between solutions. For films containing DNA (6-FAM or unmodified), the anionic PE was switched with 2×10^{-6} M solution of SA or RO in water or 0.15 M NaCl pH 4.5. DNA solutions were heated for 15 min at 80–90 °C to denature the DNA, and then cooled immediately on ice for at least 30 min before use. This deposition protocol was repeated to create films with the following compositions (where the subscript number specifies the number of bilayers); $(CHI/HA)_{10}-(CHI/SA)_5-(CHI/HA)_1$ for the CHI/HA/SA films, and $(CHI/HA)_{10}-(CHI/RO)_5-(CHI/HA)_1$ for the CHI/HA/RO films. Figure 1 shows the composition of the multilayer films and gives structural information regarding the components. CHI, HA, and rinse solutions were refreshed every 10 bilayers. Annealed films were heated for 10 min at 70 °C in 0.15 M NaCl pH 4.5 or 0.10 M KCl pH 4.5, and allowed to cool to room temperature prior to dye binding experiments. To assess dye binding, films were dipped in 200 µM SB dye (in 0.10 M KCl) for 30 min unless otherwise stated. The films were rinsed with water until the washings were no longer pink. Films were allowed to dry overnight before analysis.

Figure 1. Overview of multilayer film composition. **(A)** Schematic of optimized CHI/HA/DNA film. Ten bilayers of chitosan (CHI) (red) and hyaluronan (HA) (blue) compose the base of the film. Five bilayers composed of CHI and DNA (pink) compose the DNA layers of the film. DNA can represent the incorporation of the sulforhodamine B aptamer (SA) or the 29-nt RO. The film then topped with a single bilayer of CHI and HA (capping layer). **(B)** Monomer structures of the polyelectrolytes (PEs) used in the film and structure of the target dye SB. **(C)** Sequences of RO (left) and SA (right). Sequences are shown in their predicted secondary structures: a hairpin-loop (RO) (computed by Mfold) and a G-quadruplex (SA) (Adapted from [4]).



Preparation of films for Ultraviolet-visible (UV-Vis) analysis and dye binding experiments were conducted by the above procedure (designated as the “original” protocol) however some alternative conditions were also investigated. Growth studies and dye binding experiments were also performed for films prepared by an alternative deposition method (designated as the “modified” protocol) whose rinse procedure varied from the original protocol. Rinses (R_1 and R_2) were longer ($R_1 = 1$ min, $R_2 = 5$ min) with varying volumes ($R_1 = 10$ mL, $R_2 = 12$ mL) which were changed every four uses. CHI and HA solutions were never changed. All other conditions remained the same. In addition to this, UV-Vis growth experiments were conducted for three other variations on the modified protocol; the Mulligan, the fresh-solution (FS), and the Richert adaptations. The Mulligan adaptation involved increasing the rinse solution volumes where $R_1 = 175$ mL and $R_2 = 75$ mL [43]. The FS adaptation was conducted in the exact manner as the modified protocol as outlined above, however the rinse solutions were changed with every use. The Richert adaptation increased the number of rinses and their time and volume where $R_1 = 350$ mL for 1 s, $R_2 = 60$ mL for 6 min, and $R_3 = 60$ mL for 6 min [18]. All deposition times, conditions, and frequency of solution changes remained the same. In all UV-Vis experiments an additional rinse in water (10 mL, 5 s or 1 min) to remove excess salt was added after deposition of the layer to be analyzed. Before each spectrum was taken, the films were dried under a stream of argon.

2.3. Microscopy

2.3.1. Atomic Force Microscopy (AFM)

CHI/HA/DNA films were prepared with unmodified DNA as described in Section 2.2, with the exception that dye binding experiments were performed with a SB dye concentration of 2 mM. Topography images were taken with a Ntegra AFM (NTMDT, Moscow, Russia) in tapping mode equipped with a $100 \times 100 \mu\text{m}^2$ scanner (Ntegra) and rotated monolithic Si cantilever tips (Budget Sensors; 125 μm long, 40 N/m spring constant Tap 300Al, 315 kHz resonance frequency). A minimum of two areas were sampled from each film. All AFM images were taken at room temperature on dry films.

2.3.2. Scanning Electron Microscopy (SEM)

CHI/HA/DNA films were prepared with unmodified DNA as described in Section 2.2, with the exception that CHI/HA film dye binding experiments were performed with a SB dye concentration of 2 mM. Images were taken on a Tescan VegaII XMU SEM. All SEM images were taken at room temperature on dry films that had been sputter-coated in a gold/palladium alloy using an Anatech Hummer VII Sputter-Coater (Richmond, Canada). Images were taken from the flat surface of glass substrates.

2.3.3. Fluorescent Microscopy (FM)

Annealed and unannealed CHI/HA/DNA films were prepared with unmodified DNA by the original and modified method and incubated with SB dye as described in Section 2.2. Additionally, CHI/HA/6-FAM DNA films were prepared as well by both protocols and incubated with SB dye to analyze for binding and co-localization between the DNA and dye. Throughout sample preparation and storage, samples were shielded from all light using aluminum foil to prevent dye bleaching. All FM images were taken at room temperature on dry films. Images investigating dye-DNA co-localization

and quantification of target-dye binding were taken with an EVOS[®] FL fluorescent microscope (Life Technologies, Burlington, Canada). Fluorescence of 6-FAM DNA and SB dye was imaged using the green channel ($\lambda_{\text{excitation}} = 470 \text{ nm}$, $\lambda_{\text{emission}} = 525 \text{ nm}$) and red channel ($\lambda_{\text{excitation}} = 531 \text{ nm}$, $\lambda_{\text{emission}} = 593 \text{ nm}$), respectively. Films were rinsed after incubation with the dye in 10 mL aliquots of deionized water three (original method) or five (modified method) times for 10 s. Images of the effect of annealing on dye binding were taken with an Olympus BX61 Fluorescent microscope (Tokyo, Japan) ($\lambda_{\text{excitation}} = 531 \text{ nm}$, $\lambda_{\text{emission}} = 594 \text{ nm}$) connected to a Q-imaging Retiga 2000R camera (Surrey, BC, Canada). Films were rinsed briefly after dye incubation using deionized water. Mean fluorescent intensities of the images were calculated using ImageJ. Statistical significance was analyzed in Excel using a student t-test (heteroscedastic analysis with unequal variance, 95% confidence interval). Magnification was 10 \times for all images.

3. Results and Discussion

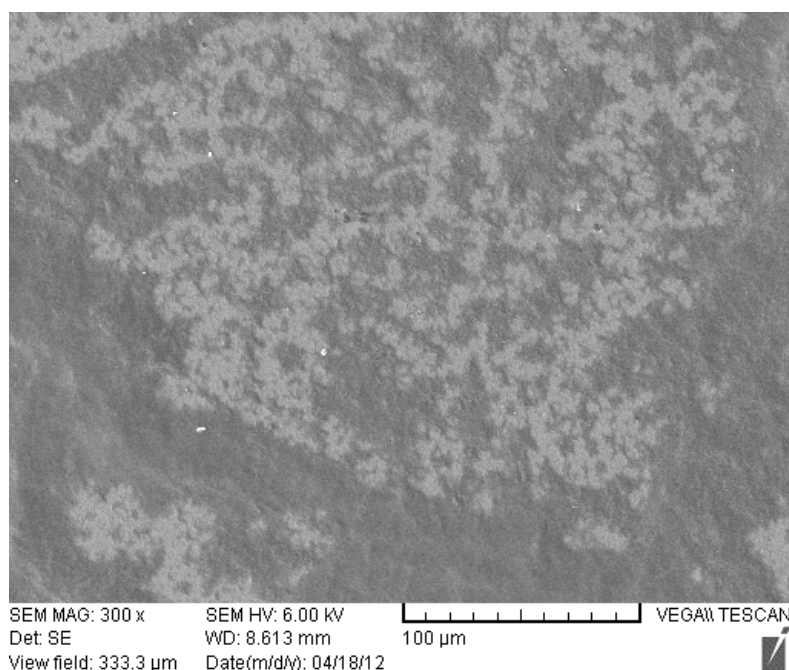
3.1. Physical Characterization of Chitosan (CHI)/Hyaluronan (HA)/DNA Films

To achieve continuous films, a base of ten CHI/HA bilayers was required to ensure a complete foundation for the deposition of the CHI/DNA bilayers. A five bilayer base proved to form porous films (not shown). Figure 2 shows a SEM image confirming the absence of pores due to the addition of ten base bilayers. The films showed identical morphology and continuity whether using SA or RO DNA as well as with or without dye exposure (not shown). AFM was used to investigate general morphology and roughness. Figure S3 shows a surface topography image of a CHI/HA/SA film which is representative of what was seen for all films imaged, however a summary of morphology properties for all films is shown in Table S1. In general, the films appear to be very rough with large microstructures arising from the island-growth mechanism of film growth. These large island peaks vary in width and height. The magnitude of the average height and the root-mean-square (RMS) roughness is indicative of an extremely rough surface, both of which vary considerably between each trial on the same film and between the different films themselves. The value of RMS roughness is affected by the inherent film characteristics (such as polyelectrolytes used), as a function of deposition conditions (such as temperature, pH, and substrate), and also by the AFM imaging conditions (such as scanning mode and rate) [44]. Despite this, RMS roughness is still a useful surface parameter and is used quite often in literature to describe CHI/HA films making it an adequate reference point.

The average RMS roughness for all films was measured to be between ~150–200 nm with very little difference between films of different DNA content and dye exposure (Table S1). The rough morphology of the films is consistent with literature for CHI/HA films. A study by Kujawa *et al.* found the RMS roughness to be ~110 nm for a hydrated 12 bilayer CHI/HA film made from 360,000 Da HA and 160,000 Da CHI [28]. The value measured in this study may have been exaggerated compared to that found by Kujawa *et al.* as the films were dried before AFM imaging, making them appear rougher. It is also unclear what affect DNA has on the film roughness. The use of ssDNA in multilayer films is uncommon. Ren *et al.* did investigate the morphology of hydrated PLL/dsDNA films and found them to form smooth films with RMS roughness values of 2.70 nm at 5 bilayers and 8.21 nm at 10 bilayers [40]. However, even at 10 bilayers the films did not form a continuous morphology but remained as the

intermediate vermiculate form. Due to the extreme variations in height and width seen in the peak-like microstructures, the thickness of the films was never measured. Hydration and swelling also play a large role in the final thickness of a film, with large differences between dry and wet films [45]. Hydrated AFM was attempted, but was never successful due to the soft nature of the films (results not shown). Thickness has been estimated for CHI/HA films by other groups for hydrated films; 869 ± 202 nm for a 12 bilayer film [28], and ~ 300 nm for a 10 bilayer film [18]. These values must not be treated as absolute measurements as PE molecular weight and deposition condition differences can affect the resulting film thickness.

Figure 2. Representative scanning electron microscopy (SEM) image from a sample set of multilayer films with the general composition of CHI/HA₁₀–CHI/DNA₅–CHI/HA₁. The image shows a rough but continuous film with no pores for a multilayer film made with SA DNA.



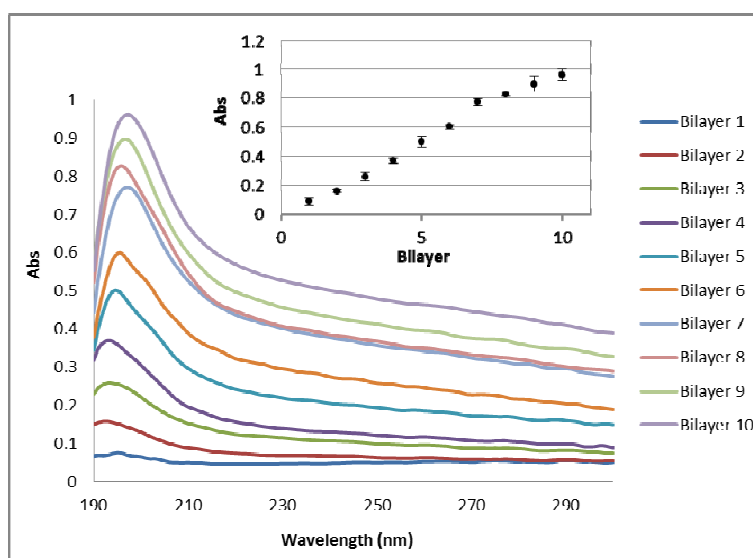
3.2. Investigation of Chitosan/Hyaluronan (CHI/HA) Film Growth by UV-Vis Spectrophotometry

The initial protocol successfully produced rough, but continuous films after the deposition of sixteen bilayers where the initial ten CHI/HA bilayers serve as a base for further growth (as discussed in Section 3.1). However, these were studies on an end product and did not shed light on the manner in which these films were growing with each additional deposition step to yield the resulting film. The growth of the CHI/HA base can be observed by UV-Vis spectrophotometry by monitoring the absorbance of glucosamine and N-acetylglucosamine which absorb between 190–220 nm [17,46,47].

The condition-set initially explored gave a linear-like growth pattern with each additional CHI/HA bilayer deposited (See Figure 3). This was unexpected as previous studies published in literature describe this system as growing exponentially [15,18,28]. Comparing published deposition conditions reveals that there is considerable variation between methods used to produce CHI/HA films (See Table 1). Previous studies have shown that polyelectrolyte molecular weight and deposition conditions play a large role in the manner in which films grow and their morphology. Richert *et al.* studied the effects of

salt concentration (0.15 , 10^{-2} , and 10^{-4} M) and the molecular weight (See Table 1) of the diffusible PE (CHI) on CHI/HA film formation [18]. Using Quartz Crystal Microbalance with Dissipation (QCM-D), the measured PE mass deposited decreased with lower salt concentrations and film growth transitioned from exponential (0.15 M) to linear (10^{-4} M). This remained true for new bilayers deposited, even if the film was previously built at higher ionic strength. Island size and thickness decreased with lower ionic strength and the transition from island to film morphology was delayed in the case of films built at 10^{-2} M NaCl compared to 0.15 M. The transition could not be achieved at all in films built at 10^{-4} M. This was attributed to the re-dissolution of unstable CHI/HA complexes due to the ionic strength of the solution. For CHI of different molecular weights, film growth remained exponential showing that the films are permeable to different PE masses. The results found by Richert *et al.* suggested the rate of growth is more rapid with smaller molecular weight species however; this was complicated by the viscoelastic properties that become dominant with CHIs of larger molecular weight [18]. Kujawa *et al.* shed further light on the effects of molecular weight in CHI/HA films finding that the growth rate did not depend on the molecular weight [28]. Molecular weight influences the transition to the exponential growth phase which in turn results in thicker films rather than a larger deposition of mass per layer formation.

Figure 3. UV-Vis spectrophotometry analysis monitoring the growth of CHI/HA bilayers deposited by the original protocol. Growth was measured by tracking the absorbance of CHI and HA between 190–220 nm. Three trials were done for each bilayer to account for minor compositional variances. An average of the three spectra is shown. Water rinse was for 5 s. Inset: Plot of the average absorbance ($N = 3$) between 190–220 nm depicting the growth trend of the CHI/HA film. Error bars represent standard deviation.



The molecular weight of both the diffusing and non-diffusing species affects this phenomenon with larger molecular weights transitioning earlier and thereby producing thicker films after the deposition of a given number of bilayers. This trend also holds true to the transition between island and vermiculate morphology. Despite this, lower molecular weight PEs produce rougher films, with larger morphological structures. The independence of the film growth rate from molecular weight has been confirmed in other systems as well [21].

From a quick overview of the conditions listed in Table 1, it becomes clear that there are a wide variety of rinsing methods which differ in many parameters including time, volume, and frequency of solution changes. The initial method used to produce CHI/HA films involved short rinsing times, in small volumes of rinse solution (0.15 M NaCl pH 4.5) which were infrequently changed; a much different protocol from those used in the literature. Rinse times were increased ($R_1 = 1$ min, $R_2 = 5$ min) and volumes changes slightly ($R_1 = 10$ mL, $R_2 = 12$ mL) in order to better emulate the literature protocols (the modified protocol). Rinse solutions were also changed more frequently. The water rinse (10 mL) time was also lengthened (1 min). Figure 4a shows the resulting growth curve for CHI/HA films produced by this method. The linear-like growth seen before was replaced by a more exponential-type growth.

A variation on the modified protocol where the rinse solutions were changed on each use was also studied (FS method). Previous studies showing exponential growth in CHI/HA films employed techniques such as QCM-D and SPR which have alternative protocols from the specified dipping method to suit the apparatus [18,28]. Because of the nature of these techniques, fresh solutions are often used in each deposition step. A ten second water rinse was performed before each scan. Figure 4b shows the resulting growth curve from this method. The exponential-like growth was very similar to the results obtained from the modified protocol, with the exception that a smaller mass of PE was deposited per deposition cycle. The onset of the exponential growth phase is slightly delayed as a result of the additional washes.

Another variation, modeled after the Mulligan *et al.* protocol, involved increasing the rinse volumes used [43]. The original protocol parameters used are listed in Table 1. Mulligan *et al.* used glass coverslip substrates which were 25 mm \times 25 mm (from personal communication) which were approximately twice the size of the slides employed in these studies. Therefore, the original rinse volumes used were scaled down by half ($R_1 = 175$ mL and $R_2 = 75$ mL). A water rinse (1 min) was performed before each scan. Figure 4c shows the resulting growth curve from this protocol. An exponential-like growth trend was seen across all ten bilayers deposited. Compared to the modified method films, the mass of polyelectrolyte deposited per deposition cycle is much lower.

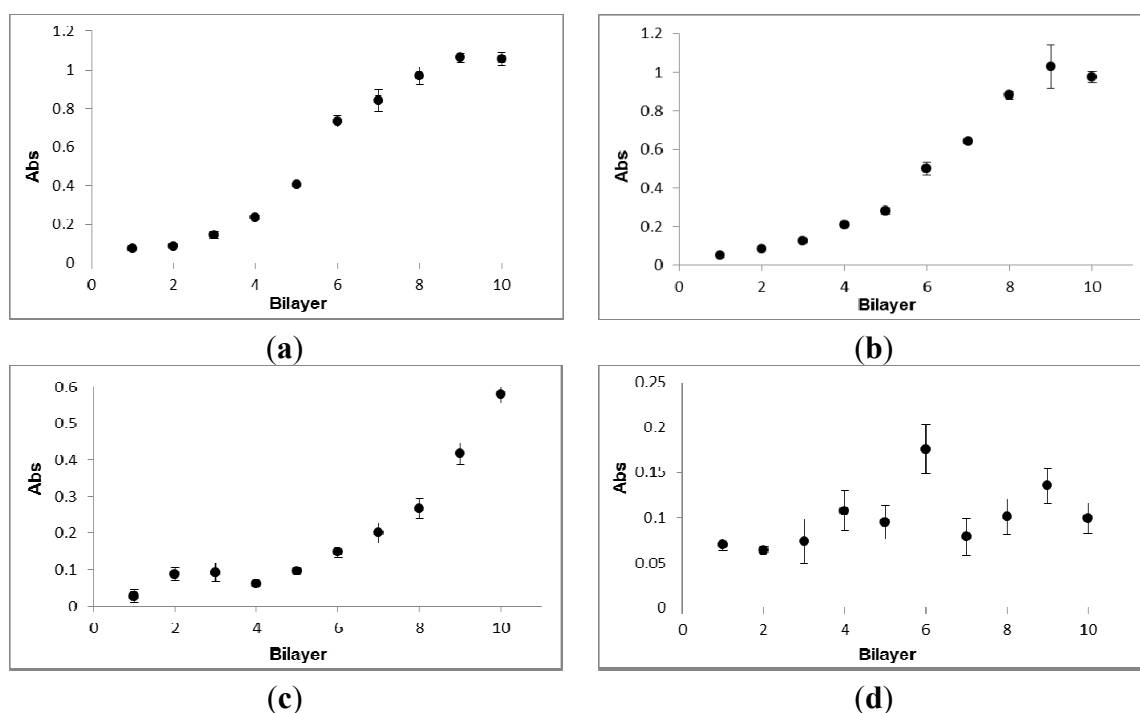
Finally, one last variation on the rinse procedure was explored. This was modeled after the protocol used by Richert *et al.* (See Table 1) [18]. In this method, both rinse volume and the number of rinses increased compared to the modified method. As the substrate size used was unclear, the solution volumes were not changed from the original protocol. A ten second water rinse was performed before each scan. Figure 4d shows the resulting growth curve. No visible trends could be discerned. The rinse procedure used by Richert *et al.* is much more intense than any protocol used previously and has already proven to successfully yield continuous CHI/HA films after ten bilayers [18]. Because of this, the amount of PE deposited is reduced below the detection threshold of the UV-Vis spectrophotometer.

Table 1. Review of deposition conditions from literature comparing key parameters of chitosan (CHI)/hyaluronan (HA) film experiments [18,27–29,43]. Asterisks (*) show conditions with confirmed exponential growth.

Group	Technique (s)	Deposition Time (min)	PE Volume (mL)	PE Change Frequency	Rinse Times	Rinse volume (mL)	Rinse Change Frequency	PE Molecular weight (g/mol)
Foster	<ul style="list-style-type: none"> • UV-Vis • Hand-dipped 	15	10	20 layers	$R_1 = 10$ s $R_2 = 5$ s	$R_1 = 10$ $R_2 = 10$	20 layers	HA = 1,580,000 CHI = 135,000
Mulligan	<ul style="list-style-type: none"> • AFM • Ellipsometry 	15	Not specified	Not specified	$R_1 = 1$ min $R_2 = 5$ min	$R_1 = 350$ $R_2 = 150$	3 layers	HA = 163,000 CHI = 50,000
Kujawa *	<ul style="list-style-type: none"> • SPR • AFM 	20	10 (total)	Each use	Not specified	10 (total)	Each use	HA ₁ = 360,000 HA ₂ = 31,000 CHI ₁ = 160,000 CHI ₂ = 30,000
Picart	<ul style="list-style-type: none"> • ATR-FTIR • CLSM • QCM • Auto-dipped 	15	12	Not specified	$R_1 =$ dip $R_2 = 2.5$ min $R_3 = 2.5$ min	$R_1 = 350$ $R_2 = 40$ $R_3 = 40$	6 layers	HA = 400,000 CHI ₁ = 5,000 CHI ₂ = 100,000
Schneider	<ul style="list-style-type: none"> • AFM • CLSM • Auto-dipped 	15	12	Not specified	$R_1 =$ dip $R_2 = 2.5$ min $R_3 = 2.5$ min	$R_1 = 350$ $R_2 = 40$ $R_3 = 40$	6 layers	HA = 400,000 CHI = 5,000
Richert *	<ul style="list-style-type: none"> • OWLS • AFM • QCM-D • Auto-dipped 	15	15 or 0.5 (QCM-D)	Not specified or each use (QCM-D)	$R_1 =$ dip $R_2 = 6$ min $R_3 = 6$ min or 10s (QCM-D)	$R_1 = 350$ $R_2 = 40$ $R_3 = 40$ or 0.5 (QCM-D)	3 layers or each use (QCM-D)	HA = 400,000 CHI ₁ = 110,000 CHI ₂ = 270,000 CHI ₃ = 460,000

AFM: Atomic Force Microscopy; SPR: Surface Plasmon Resonance; ATR-FTIR: Attenuated Total Reflectance-Fourier Transform Infrared Spectroscopy; CLSM: Confocal Laser Scanning Microscopy; QCM: Quartz Crystal Microbalance; OWLS: Optical Waveguide Lightmode Spectroscopy; QCM-D: Quartz Crystal Microbalance with Dissipation.

Figure 4. Plot of the average absorbance between 190–220 nm monitoring the growth of chitosan (CHI)/hyaluronan (HA) bilayers deposited by adaptations of the original protocol. Three trials were done for each bilayer to account for minor compositional variances. Water rinse was for 1 min. Error bars represent standard deviation. The following variations of the original protocol were performed: (a) Increased rinse times, volume, and frequency of solution changes (modified protocol); (b) Modified protocol where rinses were changed with every use (FS protocol); (c) Modified protocol with increased rinse volumes (Mulligan protocol); and (d) Modified protocol with increased rinse volume, time, and number of rinses (Richert protocol).



Richert *et al.* monitored film growth using AFM which is an extremely sensitive instrument and can detect very small changes [18]. The UV-Vis cannot compete with this level of sensitivity.

From the experiments performed, it appears that restricting rinse time during all stages of deposition yields a linearly growing film. If the rinse time is lengthened (constant volume) a more exponential-like growth is seen even with reduced volume. The main outcome of a short rinsing time is an excess of polyelectrolyte; mainly CHI due to its ability to diffuse into the film matrix. After incubation in the CHI solution, the film will be saturated with free or loosely associated CHI. Normally over the course of longer rinse times; some of the CHI would diffuse out of the film until a large enough energy barrier (electrochemical) builds to stop further diffusion [18]. The amount of CHI that diffuses in and out of a film has not yet been investigated. In shortened rinse times, CHI is not given enough time to diffuse out of the film and thus the film remains saturated into the next deposition cycle. Under the time constraints of the next incubation with HA, the entire reservoir of free CHI will not be complexed with HA and some will remain in the film. This reservoir will persist and grow with subsequent deposition steps forming a “trapped” population of CHI. During the next deposition cycle, the film is “topped-up” with CHI and the already sequestered CHI from the previous deposition round remains trapped. Therefore, the same amount of CHI will be deposited in each deposition cycle.

A concept similar to this has already been proposed twice, first by Hubsch *et al.* and then by Salomaki *et al.* for film systems exhibiting a transition from exponential to linear growth patterns [25,48]. Several studies have shown that exponentially growing films will exhibit linear growth after the deposition of ten or more bilayers [21,25,48–50]. It was theorized that exponentially growing films become too thick and evolve three distinct domains within their architecture: Domain I which is in contact with the substrate, Domain III which is at the solution interface and remains permeable to diffusing PE, and eventually Domain II (restructuring zone) which lies between Domains I and III and is constantly in a state of re-organization to a denser film structure making it impermeable to diffusing PE [21,25,48,49]. As a diffusing PE can only permeate so far in a finite amount of time, the film begins to grow linearly [47]. The presence and dense structure of Domain II helps to enforce linear growth. Porcel *et al.* studied this idea with two other exponentially growing film systems; HA/PLL and PGA/PAH [21,47]. Low molecular weight PLL (20,000 and 55,000) was able to diffuse through the entire film structure regardless of the PLL molecular weight used to build the film, while high molecular weight PLL (360,000) was restricted to a diffusion zone of approximately 4 μm in all film types (HA held constant at 400,000) [21]. While these results complicate the current hypothesized model, the factors influencing the exponential to linear transition are still not fully understood and investigation is on-going. Porcel *et al.* hypothesized that diffusion may still be an active process in the linear growth regime however the complexes free PLL forms with HA during the next deposition cycle may be unstable and only a fraction will remain associated with the film at the solution interface [21].

The molecular weight of CHI used is within the same range as the high molecular weight PLL used in the discussed study and is expected to have more limitations with diffusing into a film matrix. CHI also is a relatively stiff, extended molecule (persistence length of 6–12 nm) which also will contribute to its diffusion behavior due to steric constraints [18]. The diffusion profile seen in the high molecular weight model studied by Porcel *et al.* was constant for up to one week lending support to the hypothesis that a population of PE can remain sequestered within a film [21]. Drying was shown not to effect the growth of modified method films (results not shown), however it was never investigated for this procedure. It is possible that the drying process affects the natural diffusion behavior by forcing the film to adopt a dense structure. Depending on the speed of restructuring, the film may not have time (in solution) to re-establish the preferred hydrated morphology. This has been a concern of more than one author studying the exponential to linear transition; however it was ruled out by Porcel *et al.* who saw no changes in growth rate, mechanism, and film thickness [49]. Despite this revelation, the films used were constructed by a spray method rather than dipping and could be the result of the deposition procedure. Other procedure-dependent trends have been noted with regard to film growth [21]. It is also possible that the linearly-built films are only stable as long as conditions permit an abundance of CHI within the film matrix, and will lose mass if left in a buffered solution as a new equilibrium becomes established.

The rinsing step serves to prevent contamination of the dipping solutions by removing excess and weakly held PE chains. Therefore, the observed decrease in apparent film growth with increased rinse intensity may also be a reflection on the interactions between CHI and HA. This film system is generally regarded as a “weak” PE pair and thus may be less resilient to aggressive rinse protocols leading to larger material losses during rinsing. Regardless, it has become a common practice to

classify film pairs into “linear” and “exponential” growth types based on their intrinsic properties however, it must be recognized that the growth patterns seen are also to some extent a reflection of the chosen conditions. An intimate understanding of the physical changes that occur in films as a result of environmental and depositional conditions is required for future smart material applications to succeed. It is obvious from the growth studies that LBL film formation is sensitive to the experimental conditions which could prove challenging for production of consistent and reproducible products. However, with further knowledge of the resulting outcomes, these properties can be used to carefully optimize construction protocols and further tailor films to have the desired characteristics.

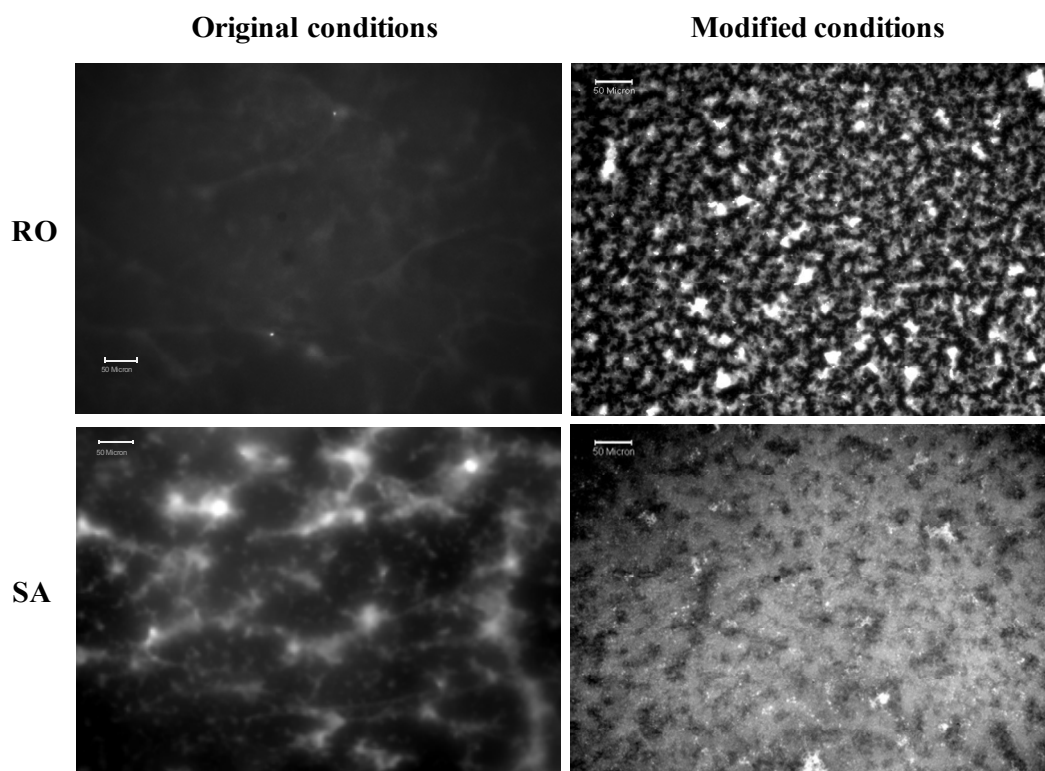
3.3. Fluorescent Microscopy (FM) Analysis of Aptamer-Target Binding

3.3.1. Original Method vs. Modified Method

The effects of changing rinse times and volumes appear to have considerable effects on the interaction of the films with the target dye (Figure 5). Films produced by the modified method show an increased level of dye binding. This binding is most likely nonspecific in nature due to the differences seen in dye binding between films containing RO DNA which has been shown to have no affinity for the target dye in the proof of concept work [36,37]. SB dye is negatively charged and therefore will inevitably have some interaction with the films due to the nature of their construction.

The increased rinse times employed in the modified deposition method may result in less PE composing the film network forming a film that is less dense and sterically hindered, allowing the dye increased access to the film interior. Within the film, the dye may be able to displace the ions neutralizing fixed positive charges and assume their counter-active role, thus interacting nonspecifically (electrostatically) with the film matrix. This argument is appealing especially since the fluorescent images strongly resemble the optical and SEM image taken of the films and show distinct morphological features (See Figure 2). Studies of the diffusion behavior of counter-ions within linear and exponentially growing films are complicated and often contradictory. A more recent study by Ghostine *et al.* with PSS/PDDA films addresses a lot of the current issues in this field. Among other things, they found after the deposition of 12–14 bilayers, PSS is no longer able to compensate for all positive charges of PDDA [51]. As a result, counter-ions from the surrounding solution must permeate the film to neutralize these fixed charges. This transition may occur sooner in CHI/HA films. PSS is likely superior to HA at compensating positive charges as every monomer is charged, whereas the repeated unit of HA consists of one charged and one uncharged group. Despite the increase in nonspecific binding seen in the modified method films, the trends in dye binding seem to be similar with the original method films in those films prepared with SA DNA showing more interaction with the target dye than films prepared with RO DNA.

Figure 5. Comparison of SB dye binding in chitosan (CHI)/hyaluronan (HA)/DNA films with either random oligomer (RO) (top) or SA (bottom) after exposure to 200 μ M SB dye. Images were taken by FM ($\lambda_{em} = 594$ nm) tracking the fluorescence of SB dye. Films were prepared by the original method (left) and modified method (right) of deposition and were imaged dry. Scale bar, 50 μ m.



3.3.2. Target Dye Binding—Original Method

FM was also used to determine the ability of SA to bind SB dye while sequestered in a film matrix. While the presence of SB dye in the films was confirmed (as discussed previously), these results did not shed light on the relative location of the DNA or confirm the co-localization of both species within the film. Using fluorescently labeled DNA, SB dye was found in the same regions as the DNA within the CHI/HA/SA films and to a lesser extent in the CHI/HA/RO films indicating that the presence of dye within the films solely due to nonspecific interactions is unlikely (Figure 6). The mean fluorescence from each channel was calculated using ImageJ (National Institutes of Health, Bethesda, MD, USA) and expressed as a ratio to quantify the dye bound by each film (Figure 7). The ratio of dye to DNA was significantly higher for the CHI/HA/SA film ($p = 0.0008$, $\alpha = 0.05$) confirming the ability of the aptamer to bind its target within a film matrix. Interestingly, all FM images analyzed indicated a higher loading of RO DNA within the films as compared to SA DNA. This may be due to the conformational differences between the two sequences that result in structural consequences within a film. RO is much less structured than SA which folds into a G-quadruplex (See Figure 1). This extended conformation may have more charges available for interaction with the PE network in the film compared to the G-quadruplex. The size difference between the DNA and the PEs could also contribute to this effect. Both SA and RO are quite small (9225 Da and 8940 Da for SA and RO

respectively) compared to the PEs used in this experiment (See Table 1). The G-quadruplex structure transforms this small DNA polymer into an even smaller, more compact entity. This may allow SA DNA to diffuse from the film more readily especially if the structure is already loosely associated with the film matrix due to the limited availability of charges. As it is unclear whether binding induces a conformational change in an aptamer or the sequence is pre-folded [52], it is possible that the conformational change induced in SA upon target binding allows for the escape of DNA-target complexes. This could be through a combination of conformational compactness and competition with the film matrix for interaction with the aptamer sequence. This is further supported by control films prepared with 6-FAM DNA for CHI/HA/RO and CHI/HA/SA films which do not show the same depositional bias (images not shown).

Figure 6. Representative fluorescent microscopy (FM) images of chitosan (CHI)/hyaluronan (HA)/fluorescein (6-FAM) DNA multilayer films exposed to 200 μ M SB dye showing co-localization (Fluorescein-Sulforhodamine B (SB) overlay; orange) of DNA (Fluorescein; green) and SB dye (SB dye; red) fluorescence as an indication of binding. Films contain either RO DNA (left) or sulforhodamine B aptamer (SA) DNA (right). Films were prepared using the original method of deposition. Scale bar, 400 μ m.

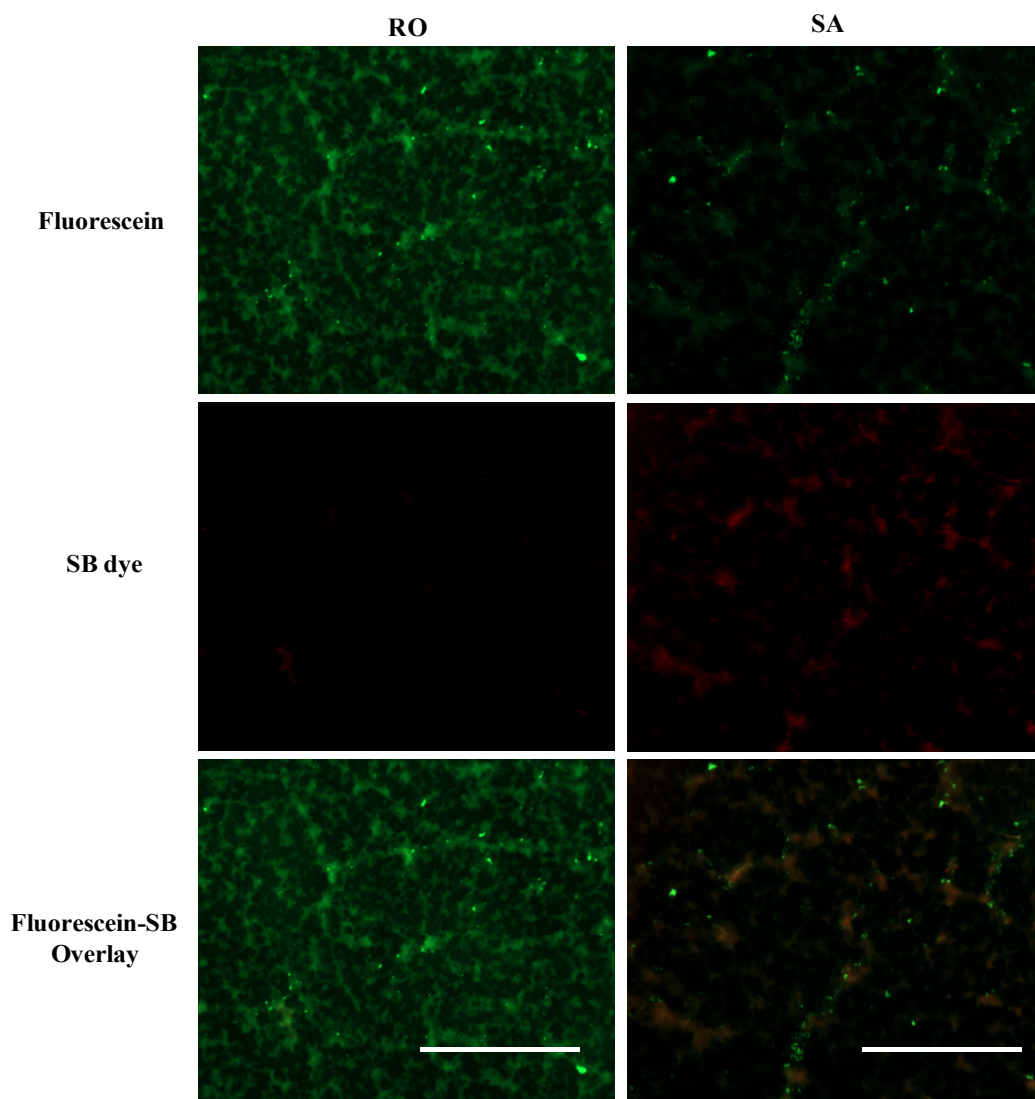
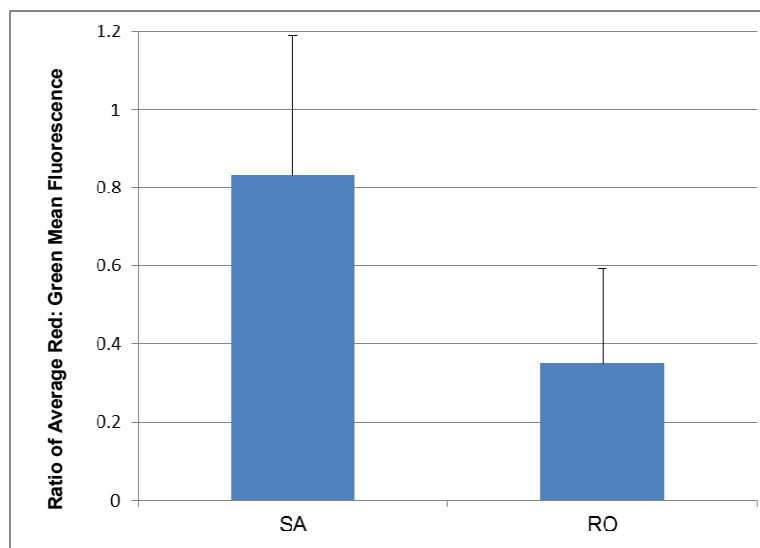


Figure 7. Chitosan Comparison of the average red: green channel mean fluorescence ratio between chitosan (CHI)/hyaluronan (HA)/fluorescein (6-FAM) DNA films containing either sulforhodamine B aptamer (SA) or RO DNA ($N = 11$) as an indication of binding. Films were prepared by the original method of deposition and exposed to 200 μM SB dye. Error bars represent standard deviation. Difference between the ratios is statistically significant ($p < 0.05$).



3.3.3. Target Dye Binding—Modified Method

The same process was repeated for films prepared by the modified method with much different results. No co-localization could be determined due to the extensive interaction between the SB dye and the film matrix (Figure 8). This was further confirmed by calculating the dye to DNA ratio (Figure 9) which yielded ratios that had no significant difference ($p = 0.3742$, $\alpha = 0.05$) between the CHI/HA/SA and CHI/HA/RO films and large standard deviations. Interestingly, clear pockets can be seen in the red channel images for both film types which perfectly coincide with the locations of DNA fluorescence (Figure 8). Fluorescence of the SB dye could be blocked by the presence of DNA leading to the darker color (reduced fluorescent intensity) of these pockets. The differences seen between the original and modified method films can be attributed to the differences in PE film density as discussed previously. Dye is seen only in the regions inhabited by DNA in the films prepared by the original method which arise from binding events. In the modified method films, the decreased steric limitations on film permeability allow the dye increased access to the film and the nonspecific interactions that occur prevent or mask any binding events that (could) occur. As in the original method films, the RO sequence was again seen in higher levels than SA in the films.

Figure 8. Representative FM images of chitosan (CHI)/hyaluronan (HA)/fluorescein (6-FAM) DNA multilayer films exposed to 200 μ M SB dye showing co-localization (Fluorescein-sulforhodamine B (SB) overlay; orange) of DNA (Fluorescein; green) and SB dye (SB dye; red) fluorescence as an indication of binding. Films contain either RO DNA (left) or sulforhodamine B aptamer (SA) DNA (right). Films were prepared using the modified method of deposition. Scale bar, 400 μ m.

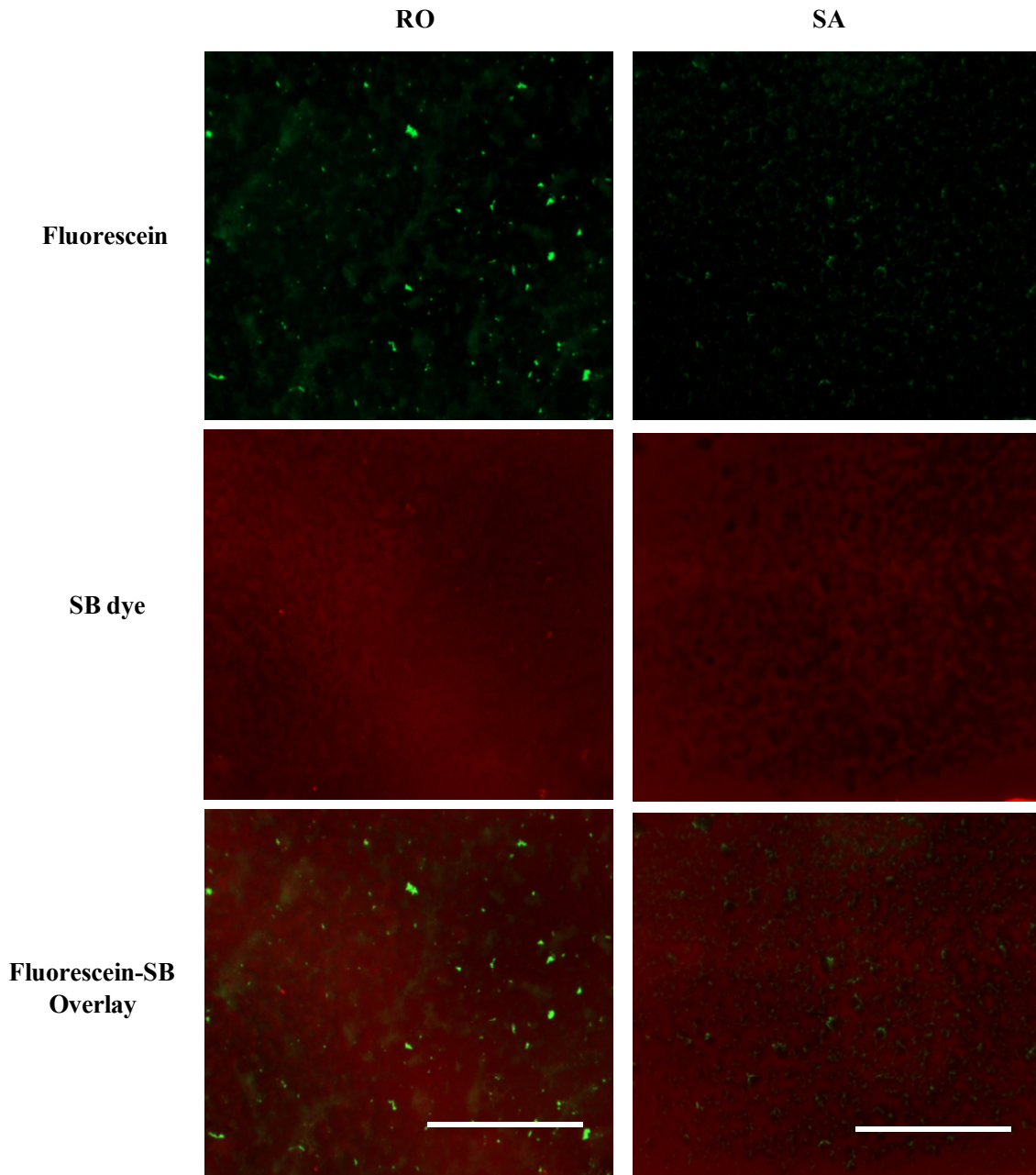
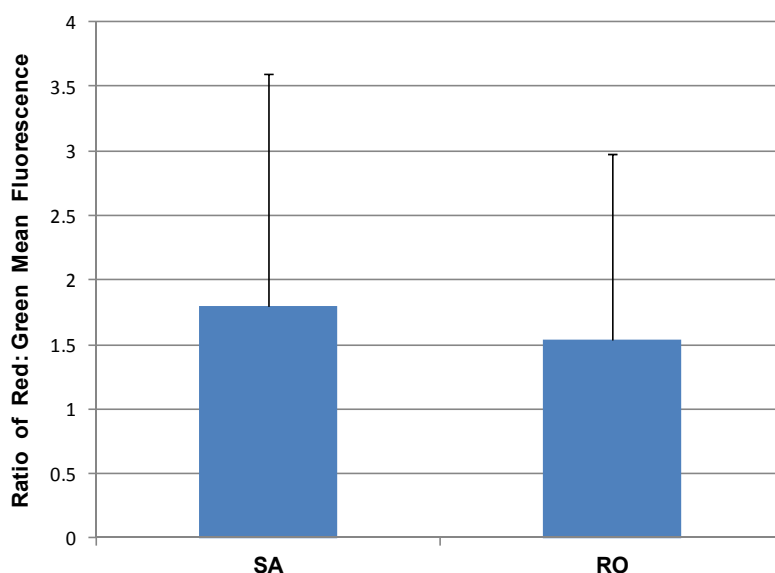


Figure 9. Comparison of the average red: green channel mean fluorescence ratio between chitosan (CHI)/hyaluronan (HA)/fluorescein (6-FAM) DNA films containing sulforhodamine B aptamer (SA) or RO DNA ($N = 8$) as an indication of binding. Films were prepared by the modified method of deposition and exposed to 200 μM sulforhodamine B (SB) dye. Error bars represent standard deviation.



4. Conclusions

Through FM analysis, it was shown that the SB aptamer could retain its binding function within a CHI/HA film matrix. Rinsing conditions proved to have a large effect on film growth, DNA distribution, and aptamer-dye interaction. Increasing the rinse time and volume was found to transition film growth from linear to a more exponential-like growth. Short rinsing times yielded linearly growing films with “hotspots” of aptamer-dye interaction that are significantly higher than films built with the RO control sequence. Longer rinsing times result in films with a more exponential-like growth, however the increase in nonspecific interaction between the dye and film matrix masked any aptamer-dye binding that may be occurring. While UV-Vis spectrophotometry gives an adequate preliminary analysis, more sensitive techniques such as QCM-D and AFM would lend further information in examining the impact of rinse time and volume on film growth and morphology. This would also allow a better investigation into the manner of growth in CHI/DNA films whose growth fell below the detection limits of the UV-Vis spectrophotometry (results not shown). The research presented demonstrates that a highly structured aptamer can still function within a CHI/HA film matrix, confirming the observations from the previous proof of concept work with PSS/PDDA and PSS/PAH. This promising result likely translates to many film systems and opens doors to the large number of PEs available for LBL film assembly; providing a wide range of materials and functionalities to tailor smart material systems to meet the specific characteristics required for their intended purpose. Moreover, this system confirmed the applicability of aptamers to materials possessing the desired biocompatibility properties which could prove useful in many controlled release applications such as therapeutics and agriculture. Future work will investigate the matrix effect on aptamer specificity and on the development of microcapsule systems.

Acknowledgments

The authors would like to thank Matthew Holahan and Sabrina Dawson for all their help in with the fluorescent microscope images as well as Amy Won for help with the AFM images and all help with their analysis. Amanda Foster acknowledges the Natural Sciences and Engineering Council (NSERC) for funding through a Canada Graduate Scholarship. Maria C. DeRosa acknowledges NSERC, the Canada Foundation for Innovation (CFI), the Ontario Ministry of Research and Innovation (MRI), and Alberta Innovates Biosolutions (AIBS) for funding. Maria C. DeRosa acknowledges Carlos Monreal and Agriculture and Agri-food Canada for discussions on the project.

Author Contributions

Amanda Foster designed, performed, and analyzed the experiments and wrote the manuscript. Maria C. DeRosa conceived, designed and analyzed the experiments and edited the manuscript.

Conflicts of Interest

The authors declare no conflict of interest.

References

1. Decher, G. Fuzzy nanoassemblies: Towards layered polymeric multicomposites. *Science* **1997**, *277*, 1232–1237.
2. Zasadzinski, J.A.; Viswanathan, R.; Madsen, L.; Garnæs, J.; Schwartz, D.K. Langmuir-blodgett films. *Science* **1994**, *263*, 1726–1733.
3. Crawford, N.F.; Leblanc, R.M. CdSe and CdSe (ZnS) quantum dots in 2D: A Langmuir monolayer approach. *Coord. Chem. Rev.* **2014**, *263*, 13–24.
4. Ariga, K.; Yamauchi, Y.; Mori, T.; Hill, J.P. 25th anniversary article: What can be done with the langmuir-blodgett method? Recent developments and its critical role in material science. *Adv. Mater.* **2013**, *25*, 6477–6512.
5. Ariga, K.; Yamauchi, Y.; Rydzek, G.; Ji, Q.; Yonamine, Y.; Wu, K.C.W.; Hill, J.P. Layer-by-layer nanoarchitectonics: Invention, innovation, and evolution. *Chem. Lett.* **2014**, *43*, 36–68.
6. Yan, Y.; Bjornmalm, M.; Caruso, F. Assembly of layer-by-layer particles and their interactions with biological systems. *Chem. Mater.* **2014**, *26*, 452–460.
7. Deshmukh, P.K.; Ramani, K.P.; Singh, S.S.; Tekade, A.R.; Chatap, V.K.; Patil, G.B.; Bari, S.B. Stimuli-sensitive layer-by-layer (LBL) self-assembly systems: Targeting and biosensory applications. *J. Control. Release* **2013**, *166*, 294–306.
8. Ariga, K.; Ji, Q.; Hill, J.P.; Bando, Y.; Aona, M. Forming nanomaterials as layered functional structures toward materials nanoarchitectonics. *NPG Asia Mater.* **2012**, *4*, doi:10.1038/am.2012.30.
9. Li, C.; Ma, C.; Wang, F.; Xi, Z.; Wang, Z.; Deng, Y.; He, N. Preparation and biomedical applications of core-shell silica/magnetic nanoparticle composites. *J. Nanosci. Nanotechnol.* **2012**, *12*, 2964–2972.
10. Joseph, N.; Ahmadiannamini, P.; Hoogenboom, R.; Vankelecom, I.F.J. Layer-by-layer preparation of polyelectrolyte multilayer membranes for separation. *Polym. Chem.* **2013**, *5*, 1817–1831.

11. Kharlampieva, E.; Sukhishvili, S.A. Hydrogen-bonded layer-by-layer polymer films. *J. Macromol. Sci. C Polym.* **2006**, *46*, 377–395.
12. Sievers, T.K.; Vergin, A.; Mohwald, H.; Kurth, D.G. Thin film of cross-linked metallo-supramolecular coordination polyelectrolytes. *Langmuir* **2007**, *23*, 12179–12184.
13. Kotov, N.A. Layer-by-layer self-assembly: The contribution of hydrophobic interactions. *Nanostruct. Mater.* **1999**, *12*, 789–796.
14. Schoeler, B.; Kumaraswamy, G.; Caruso, F. Investigation of the influence of polyelectrolyte charge density on the growth of multilayer thin films prepared by the layer-by-layer technique. *Macromolecules* **2002**, *35*, 889–897.
15. Lavalle, P.; Picart, C.; Mutterer, J.; Gergely, C.; Reiss, H.; Voegel, J.C.; Senger, B.; Schaaf, P. Modeling the buildup of polyelectrolyte multilayer films having exponential growth. *J. Phys. Chem.* **2004**, *108*, 635–648.
16. Lvov, Y.; Decher, G.; Mohwald, H. Assembly, structural characterization, and thermal behavior of layer-by-layer deposited ultrathin films of poly(vinyl sulfate) and poly(allylamine). *Langmuir* **1993**, *9*, 481–486.
17. Mesquita, J.P.; Donnici, C.L.; Pereira, F.V. Biobased nanocomposites from layer-by-layer assembly of cellulose nanowhiskers with chitosan. *Biomacromolecules* **2010**, *11*, 473–480.
18. Richert, L.; Lavalle, P.; Payan, E.; Shu, X.Z.; Prestwich, G.D.; Stoltz, J.F.; Schaaf, P.; Voegel, J.C.; Picart, C. Layer by layer buildup of polysaccharide films: physical chemistry and cellular adhesion aspects. *Langmuir* **2004**, *20*, 448–458.
19. Elbert, D.L.; Herbert, C.B.; Hubbell, J.A. Thin polymer layers formed by polyelectrolyte multilayer techniques on biological surfaces. *Langmuir* **1999**, *15*, 5355–5362.
20. Picart, C.; Lavalle, P.; Hubert, P.; Cusinier, F.J.G.; Decher, G.; Schaaf, P.; Voegel, J.C. Buildup mechanism for poly(L-lysine)/hyaluronic acid films onto a solid surface. *Langmuir* **2001**, *17*, 7414–7424.
21. Porcel, C.; Lavalle, P.; Decher, G.; Senger, B.; Voegel, J.C.; Schaaf, P. Influence of the polyelectrolyte molecular weight on exponentially growing multilayer films in the linear regime. *Langmuir* **2007**, *23*, 1898–1904.
22. Picart, C.; Gergely, C.; Arntz, Y.; Voegel, J.C.; Schaaf, P.; Cuisinier, F.J.G.; Senger, B. Measurement of film thickness up to several hundreds of nanometers using optical waveguide lightmode spectroscopy. *Biosens. Bioelectron.* **2004**, *20*, 553–561.
23. Shiratori, S.S.; Rubner, M.F. pH-dependent thickness behavior of sequentially adsorbed layers of weak polyelectrolytes. *Macromolecules* **2000**, *33*, 4213–4219.
24. Bieker, P.; Schonhoff, M. Linear and exponential growth regimes of multilayers of weak polyelectrolytes in dependence on pH. *Macromolecules* **2010**, *43*, 5052–5059.
25. Salomaki, M.; Vinokurov, I.A.; Kankare, J. Effect of temperature on the buildup of polyelectrolyte multilayers. *Langmuir* **2005**, *21*, 11232–11240.
26. Wilson, C.; Szostak, J.W. Isolation of a fluorophore-specific DNA aptamer with weak redox activity. *Chem. Biol.* **1998**, *5*, 609–617.
27. Schneider, A.; Richert, L.; Francius, G.; Voegel, J.C.; Picart, C. Elasticity, biodegradability and cell adhesive properties of chitosan/hyaluronan multilayer films. *Biomed. Mater.* **2007**, *2*, 45–51.

28. Kujawa, P.; Moraille, P.; Sanchez, J.; Badia, A.; Winnik, F.M. Effect of molecular weight on the exponential growth and morphology of hyaluronan/chitosan multilayers: A surface plasmon resonance spectroscopy and atomic force microscopy investigation. *J. Am. Chem. Soc.* **2005**, *127*, 9224–9234.
29. Picart, C.; Schneider, A.; Etienne, O.; Mutterer, J.; Schaaf, P.; Egles, C.; Jessel, N.; Voegel, J.C. Controlled degradability of polysaccharide multilayer films *in vitro* and *in vivo*. *Adv. Funct. Mater.* **2005**, *15*, 1771–1780.
30. Zhu, Z.; Wu, C.; Liu, H.; Zou, Y.; Zhang, X.; Kang, H.; Yang, C.J.; Tan, W. An aptamer cross-linked hydrogel as a colorimetric platform for visual detection. *Angew. Chem.* **2010**, *122*, 1070–1074.
31. Farokhzad, O.C.; Cheng, J.; Teply, B.A.; Sherifi, I.; Jon, S.; Kantoff, P.W.; Richie, J.P.; Langer, R. Targeted nanoparticle-aptamer bioconjugates for cancer therapy *in vivo*. *PNAS* **2006**, *103*, 6315–6320.
32. Cao, Z.; Tong, R.; Mishra, A.; Xu, W.; Wong, G.C.L.; Cheng, J.; Lu, Y. Reversible cell-specific drug delivery with aptamer-functionalized liposomes. *Angew. Chem.* **2009**, *48*, 6494–6498.
33. Wu, Y.; Sefah, K.; Liu, H.; Wang, R.; Tan, W. DNA aptamer-micelle as an efficient detection/delivery vehicle toward cancer cells. *PNAS* **2010**, *107*, 5–10.
34. So, H.; Won, K.; Kim, Y.H.; Kim, B.; Ryu, B.H.; Na, P.S.; Kim, H.; Lee, J.O. Single-walled carbon nanotube biosensors using aptamers as molecular recognition elements. *J. Am. Chem. Soc.* **2005**, *127*, 11906–11907.
35. Mastronardi, E.; Foster, A.; Zhang, X.; DeRosa, M.C. Smart materials based on DNA aptamers: Taking aptasensing to the next level. *Sensors* **2014**, *14*, 3156–3171.
36. Sultan, Y.; Walsh, R.; Monreal, C.; DeRosa, M. Preparation of functional aptamers films using layer-by-layer self-assembly. *Biomacromolecules* **2009**, *10*, 1149–1154.
37. Sultan, Y.; DeRosa, M. Target binding influences permeability in aptamer-polyelectrolyte microcapsules. *Small* **2011**, *7*, 1219–1226.
38. Malile, B.; Chen, J.I.L. Morphology-based plasmonic nanoparticle sensors: Controlling etching kinetics with target-responsive permeability gate. *J. Am. Chem. Soc.* **2013**, *135*, 16042–16045.
39. Du, Y.; Chen, C.; Li, B.; Zhou, M.; Wang, E.; Dong, S. Layer-by-layer electrochemical biosensor with aptamer-appended active polyelectrolyte multilayer for sensitive protein determination. *Biosens. Bioelectron.* **2010**, *25*, 1902–1907.
40. Ren, K.; Ji, J.; Shen, J. Construction and enzymatic degradation of multilayered poly-L-lysine/DNA films. *Biomaterials* **2006**, *27*, 1152–1159.
41. Gu, B.X.; Xu, C.X.; Zhu, G.P.; Liu, S.Q.; Chen, L.Y.; Wang, M.L.; Zhu, J.J. Layer by layer immobilized horseradish peroxidase on zinc oxide nanorods for biosensing. *J. Phys. Chem. B* **2009**, *113*, 6553–6557.
42. He, P.; Hu, N.; Zhou, G. Assembly of electroactive layer-by-layer films of hemoglobin and polycationic poly(diallyldimethylammonium). *Biomacromolecules* **2002**, *3*, 139–146.
43. Mulligan, K.; Jakubek, Z.J.; Johnston, L.J. Supported lipid bilayers on biocompatible polysaccharide multilayers. *Langmuir* **2011**, *27*, 14352–14359.
44. Fujii, N.; Fujimoto, K.; Michinobu, T.; Akada, M.; Hill, J.P.; Shiratori, S.; Argia, K.; Shigehara, K. The simplest layer-by-layer assembly structure: Best paired polymer electrolytes with one charge per main chain carbon atom for multilayered thin films. *Macromolecules* **2010**, *43*, 3947–3955.

45. Crouzier, T.; Boudou, T.; Picart, C. Polysaccharide-based polyelectrolyte multilayers. *Curr. Opin. Colloid Interface Sci.* **2010**, *15*, 417–426.
46. Wu, T.; Zivanovic, S. Determination of the degree of acetylation (DA) of chitin and chitosan by an improved first derivative UV method. *Carbohydr. Polym.* **2008**, *73*, 248–253.
47. Liu, D.; Wei, Y.; Yao, P.; Jiang, L. Determination of the degree of acetylation of chitosan by UV spectrophotometry using dual standards. *Carbohydr. Res.* **2006**, *341*, 782–785.
48. Hubsch, E.; Ball, V.; Senger, B.; Decher, G.; Voegel, J.C.; Schaaf, P. Controlling the growth regime of polyelectrolyte multilayer films: Changing from exponential to linear growth by adjusting the composition of polyelectrolyte mixtures. *Langmuir* **2004**, *20*, 1980–1985.
49. Porcel, C.; Lavalle, P.; Ball, V.; Decher, G.; Senger, B.; Voegel, J.C.; Schaaf, P. From exponential to linear growth in polyelectrolyte multilayers. *Langmuir* **2006**, *22*, 4376–4383.
50. Michel, M.; Izquierdo, A.; Decher, G.; Voegel, J.C.; Schaaf, P.; Ball, V. Layer by layer self-assembled polyelectrolyte multilayers with embedded phospholipid vesicles obtained by spraying: Integrity of the vesicles. *Langmuir* **2005**, *21*, 7854–7859.
51. Ghostine, R.A.; Markarian, M.Z.; Schlenoff, J.B. Asymmetric growth in polyelectrolyte multilayers. *J. Am. Chem. Soc.* **2013**, *135*, 7636–7646.
52. White, R.J.; Rowe, A.A.; Plaxco, K.W. Re-engineering aptamers to support reagentless, self-reporting electrochemical sensors. *Analyst* **2010**, *135*, 589–594.

© 2014 by the authors; licensee MDPI, Basel, Switzerland. This article is an open access article distributed under the terms and conditions of the Creative Commons Attribution license (<http://creativecommons.org/licenses/by/3.0/>).